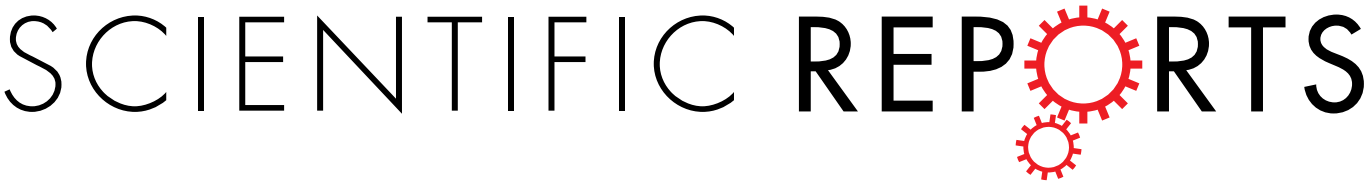

OPEN

Localized-itinerant dichotomy and unconventional magnetism in $SrRu_2O_6$

Received: 11 May 2017
Accepted: 12 July 2017
Published online: 13 September 2017

Satoshi Okamoto[1], Masayuki Ochi[2,3], Ryotaro Arita[3], Jiaqiang Yan[1] & Nandini Trivedi[4]

Electron correlations tend to generate local magnetic moments that usually order if the lattices are not too frustrated. The hexagonal compound $SrRu_2O_6$ has a relatively high Neel temperature but small local moments, which seem to be at odds with the nominal valence of Ru^{5+} in the t_{2g}^3 configuration. Here, we investigate the electronic property of $SrRu_2O_6$ using density functional theory (DFT) combined with dynamical-mean-field theory (DMFT). We find that the strong hybridization between Ru *d* and O *p* states results in a Ru valence that is closer to +4, leading to the small ordered moment ~1.2 μ_B. While this is consistent with a DFT prediction, correlation effects are found to play a significant role. The local moment per Ru site remains finite ~2.3 μ_B in the whole temperature range investigated. Due to the lower symmetry, the t_{2g} manifold is split and the quasiparticle weight is renormalized significantly in the a_{1g} state, while the renormalization in e_g' states is about a factor of 2–3 weaker. Our theoretical Neel temperature ~700 K is in reasonable agreement with experimental observations. $SrRu_2O_6$ is a unique system in which localized and itinerant electrons coexist with the proximity to an orbitally-selective Mott transition within the t_{2g} sector.

For systems with an odd number of electrons per unit cell, correlation effects can lead to insulating magnetic ground states. Depending on the relative strength between the interactions U and the electron bandwidth or kinetic energy W, there are two classes of insulators: A Slater insulator[1] in the weak coupling regime in which the normal state is a non-magnetic metal. Below a critical temperature a gap in the single-particle opens up because of magnetic ordering and consequently the unit cell gets doubled and the Brillouin zone folds up. In this regime, the magnetic transition temperature increases with increasing Coulomb interaction strength. In the opposite strong coupling regime, the system is a Mott insulator[2,3]. In this limit, the normal state is a gapped insulator due to strong Coulomb repulsion. Magnetic ordering sets in below a critical temperature $T_c \sim W^2/U$ related to the super-exchange scale[4]. Interpolating between these two limits, the maximum T_c is expected to occur in the crossover regime where U and W are comparable.

The behavior of T_c in a series of perovskite transition-metal oxides (TMOs) with the formal t_{2g}^3 electron configuration, including $SrMnO_3$, $SrTcO_3$ and $NaOsO_3$, lend support to the above picture. 3*d* TMO $SrMnO_3$ has a relatively low Néel temperature $T_N = 260$ K[5] for antiferromagnetic (AF) ordering but the insulating behavior persists above T_N, indicating that it is in the strong coupling limit. On the other hand, 5*d* TMO $NaOsO_3$ with an AF transition $T_N = 410$ K and a metal-insulator transition that is coincident[6] appears to be in the weak coupling limit. Finally, 4*d* TMO $SrTcO_3$ shows an extremely high AF $T_N \sim 1000$ K[7], which indicates it is located in the crossover regime[8]. It is also worth to note that the crossover behavior associated with high magnetic transition temperatures is realized in double perovskite TMOs $A_2BB'O_6$[9], where A is an alkali or alkaline earth metal, and B and B' are two transition metals with different Coulomb interaction strengths.

Given this backdrop, an important question that arises is *can there be systems that are incompatible with this classification?* And more broadly, what are the criteria for weak coupling Slater and strong coupling Mott regimes in multi-orbital systems?

One such systems is pyrochlore $Cd_2Os_2O_7$. As in $NaOsO_3$, the metal-insulator transition of $Cd_2Os_2O_7$ accompanies a magnetic ordering[10,11]. However, unlike $NaOsO_3$ the unit cell of $Cd_2Os_2O_7$ contains four Os sites and

[1]Materials Science and Technology Division, Oak Ridge National Laboratory, Oak Ridge, Tennessee, 37831, USA. [2]Department of Physics, Graduate School of Science, Osaka University, Osaka, 560-0043, Japan. [3]RIKEN Center for Emergent Matter Science (CEMS), Hirosawa, Wako, Saitama, 351-0198, Japan. [4]Department of Physics, The Ohio State University, Columbus, Ohio, 43210, USA. Correspondence and requests for materials should be addressed to S.O. (email: okapon@ornl.gov)

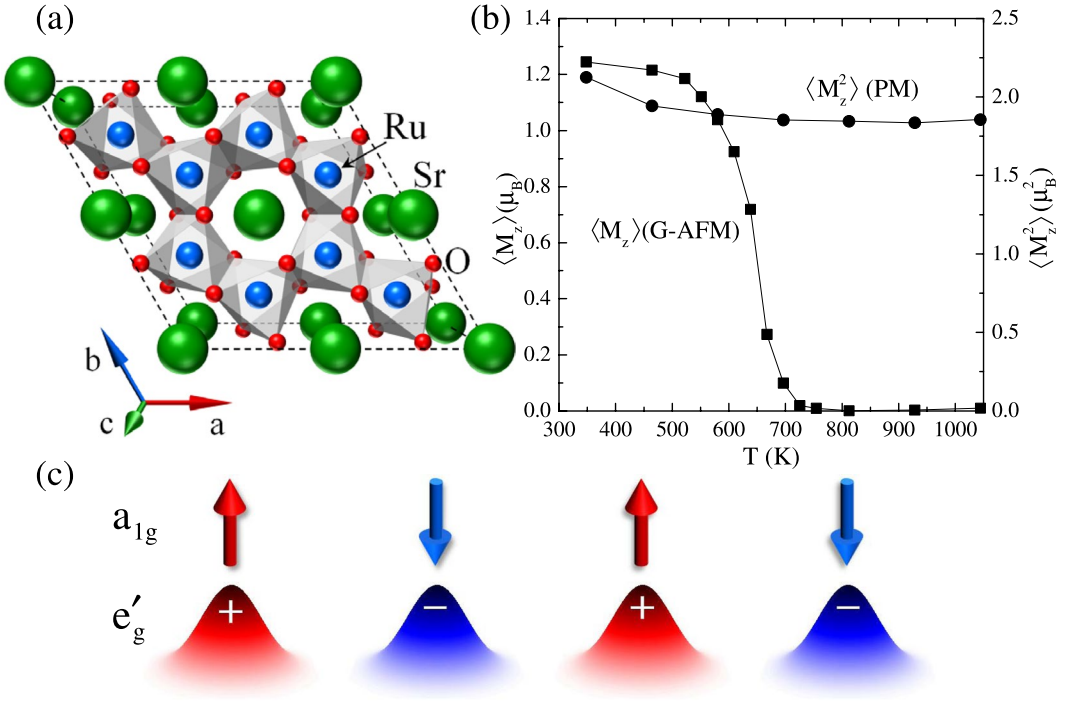

Figure 1. (**a**) Top view of $SrRu_2O_6$. The cell is doubled along the *a* and *b* directions. (**b**) Ordered $\langle M_z \rangle$ and equal-time spin-spin correlation $\langle M_z^2 \rangle$ as a function of temperature *T*. From the high temperature value, $\langle M_z^2 \rangle \sim 1.8\ \mu_B^2$, the local moment is estimated to be $M \sim 2.3\ \mu_B$. (**c**) Schematic view of the localized vs. itinerant dichotomy between a_{1g} electrons and e_g' electrons. Correlation effects are stronger for a_{1g} electrons resulting in localized moments, while e_g' electrons maintain a rather itinerant character and show spin-density wave (SDW) like behavior when magnetically ordered.

therefore can become an insulator without changing the size of the unit cell. In fact, the observed all-in-all-out magnetic structure is compatible with the structural unit cell[12,13]. It turns out that the metal-insulator transition in $Cd_2Os_2O_7$ is a Lifshitz transition[14] arising from a reconstruction of the Fermi surface, rather than a Slater transition.

In this paper, we focus on another compound, the hexagonal $SrRu_2O_6$[15] [Fig. 1(a)]. Given a half filled t_{2g} configuration for Ru sites from its formal valence +5, like Os^{5+} in $NaOsO_3$ or $Cd_2Os_2O_7$, and also because Ru is a 4*d* element, one may expect that it would show behavior similar to $SrTcO_3$. Indeed, a fairly high $T_N \sim 565$ K is observed in $SrRu_2O_6$[16]. However, the ordered moment ~1.3 μ_B is found to be much smaller than that expected for Ru^{5+}, 3 μ_B[16,17]. To solve this puzzle, there have appeared a number of theoretical studies using density functional theory (DFT). Singh[18] and Tian *et al.*[16] argued that the strong hybridization between Ru and O ions is responsible for the reduction of the ordered moment. Streltsov and coworkers proposed the formation of molecular orbitals within a Ru hexagonal plane owing to such a strong hybridization[19]. They also performed the DFT calculations combined with the dynamical mean field theory[20] (DFT + DMFT[21–23]). It was reported that the ordered moment on a Ru site becomes 3 μ_B as anticipated for Ru^{5+} and that the transition temperature becomes ~2000 K, which is very similar to a theoretical result for $SrTcO_3$[8] and in return supports the importance of the molecular orbital picture that is not considered in DMFT.

In this paper, we investigate the electronic and magnetic properties of $SrRu_2O_6$ using DFT + DMFT. Our main finding is summarized in Fig. 1(b). In contrast to the previous report of Ref.[19], we find that the ordered moment is indeed ~1.2 μ_B, which is nearly identical to the DFT result 1.3 μ_B[18] and also consistent with the experimental value 1.4 μ_B[16,17]. These observations might indicate that $SrRu_2O_6$ is in the weak coupling limit, similar to $NaOsO_3$, not in the crossover regime. However, the local moment estimated by the equal-time spin-spin correlation remains relatively large throughout the temperature range analyzed. We also find that the transition temperature estimated from DMFT is $T_N \sim 700\ K$, reasonably close to the experimental $T_N \sim 565\ K$[16,17]. Fluctuations not included in DMFT are expected to reduce the ordering temperature bringing it closer to the experimental estimate. Even more significantly, we find that one of t_{2g} states shows strong mass enhancement. Thus, our results indicate $SrRu_2O_6$ is in close proximity to an orbitally-selective Mott insulating state and localized and itinerant electrons coexist as schematically shown in Fig. 1(c).

Results

DFT analysis. We utilize DFT + DMFT techniques[21–23] to better account for correlation effects associated with the localized Ru *d* electrons. We first perform the DFT calculations for the non-magnetic state with the Elk

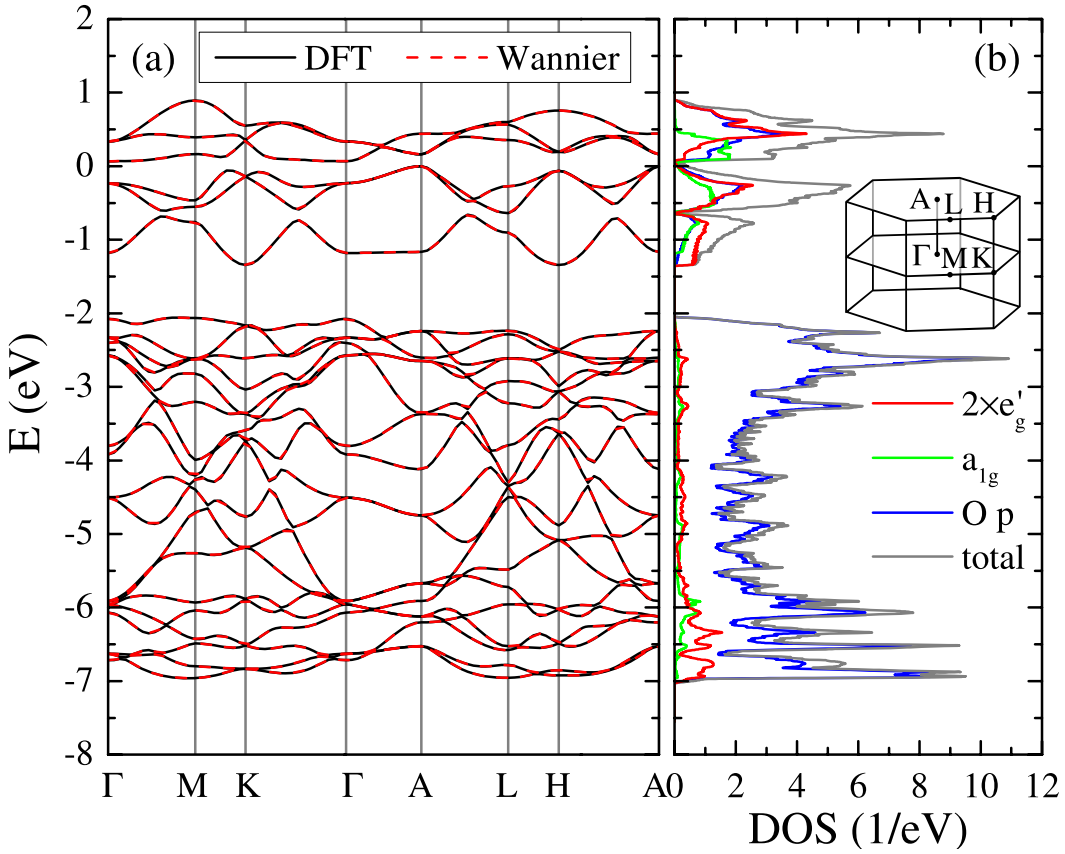

Figure 2. DFT results on $SrRu_2O_6$. (**a**) Band dispersion (solid lines) compared with Wannier dispersions (broken lines). (**b**) Total and orbital-resolved (Ru e_g', a_{1g} and O p) DOS. The valence-band maximum is set to $E=0$. DOS for e_g' involves contributions from two degenerate bands. The inset shows the first Brillouin zone for the hexagonal lattice.

package[24]. The experimental lattice parameters are considered with atomic configurations determined at room temperature[15]. It turns out that these calculations themselves provide important insights into the novel behavior of $SrRu_2O_6$. The spin-orbit coupling (SOC) λ is neglected in our analyses because $\lambda \sim 200$ meV in ruthenium oxides[25] is smaller than our estimation for the Hund coupling parameters. We anticipate that the main effect of the SOC is to introduce the uniaxial spin anisotropy.

Within the DFT, a small band gap ~0.05 eV exists at the Fermi level in a paramagnetic state[16], indicating that $SrRu_2O_6$ is a band insulator.

We then construct a model Hamiltonian consisting of Ru t_{2g} states and O p states using the Wannier functions[26–29] and transfer integrals between them on different sites extracted from the DFT band structure. We estimate the interaction parameters from the constrained random phase approximation (cRPA)[30]. Details of our model construction are provided in the Methods section. The interacting model thus obtained is solved by means of DMFT with the continuous-time quantum Monte-Carlo impurity solver[31–33].

It is instructive to start from the DFT results as summarized in Fig. 2. Figure 2(a) shows the DFT dispersion relations near the Fermi level. The valence-band maximum is set to $E=0$. The first Brillouin zone for the hexagonal lattice is shown as an inset of Fig. 2(b). In this calculation, magnetic ordering is suppressed. RuO_6 octahedra are slightly compressed along the c direction, and O-Ru-O angle is about 94.4° (two oxygen sites are on the same plane). Reflecting this distortion and the hexagonal symmetry, i.e., a_{1g} and e_g' are intrinsically inequivalent, the a_{1g} level is about 0.3 eV higher than the e_g' level in the Wannier basis.

These bands are well separated from the other bands located below −15 eV or above +3 eV. As shown in Fig. 2(b), these bands primarily come from Ru t_{2g} states (split to twofold degenerate e_g' states and non-degenerate a_{1g} states) and O p states, justifying our choice of the basis set of the model Hamiltonian. It is clearly seen that Ru t_{2g} and O p states are strongly hybridized in the energy window [−7.0: +1.0] eV, which is used to construct Wannier functions in this study. Because of this large energy window, Wannier orbitals with the t_{2g} symmetry centered on a Ru site are well localized with the typical spatial spread 1.0–1.2 Å. Interestingly, a substantial amount of O p states are above the Fermi level, corresponding to 2.596 holes in the O p states per unit cell or 0.433 holes per oxygen ion. This point will become crucial in the discussion below. It should also be mentioned that Ru a_{1g} states have the largest weight near the Fermi level (Note that Ru e_g' states have the twofold degeneracy, therefore

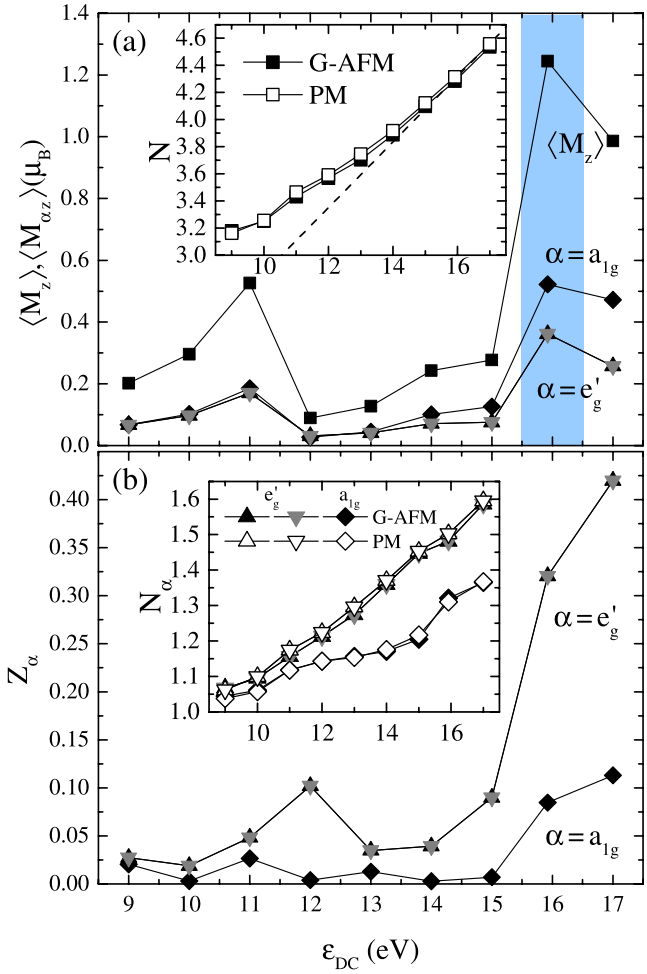

Figure 3. (**a**) DMFT results of the total and the orbital-resolved ordered magnetic moments, $\langle M_z \rangle$ and $\langle M_{\alpha z} \rangle$, respectively, as a function of ε_{DC}. (**b**) Quasiparticle weight Z_α as a function of ε_{DC}. The insets of (**a**) and (**b**) respectively show the total d electron density N and the orbital-resolved density N_α as a function of ε_{DC}.

each e_g' band has the smaller spectral weight than the a_{1g} band near the Fermi level). This indicates that the effect of correlations is different between e_g' and a_{1g} states.

Figure 2 (a) also shows the Wannier dispersion relations, which completely overlap with the DFT dispersion relations. There are 48 bands including the spin degeneracy, i.e., 6 per Ru (t_{2g}) and 6 per O (p_x, p_y, p_z). A Sr does not contribute to these low-energy bands because Sr 5s(4p) level is so high (low) and its valence state is +2 by donating 2 electrons to these bands. Considering the nominal valence, $Sr^{2+}Ru_2^{5+}O_6^{2-}$, and the charge counting, 3 per Ru^{5+} and 6 per O^{2-}, these bands are filled by 42 electrons. In this study, the orbital occupancy is determined in the Wannier basis. This is also used to determine the valence state of a Ru ion and the magnetic moment. Within DFT with the Wannier basis, the filling is about 1.42 per a_{1g} orbital and about 1.45 per e_g' orbital, so these orbitals are nearly equally filled. Since the total t_{2g} occupation 4.3 is larger than 3, the Ru valence state is deviated from the nominal value +5 to +3.7.

Double-counting correction. For methods using DFT supplemented by many-body calculations, it is critical that we first correct for the Hartree contribution arising from correlated orbitals that is already included in the DFT calculation; we call this the double-counting correction (DC). This is introduced as a uniform level shift of correlated orbitals ε_{DC}. Two methods for accounting for such a DC correction have been investigated during the development of local (spin) density approximation [L(S)DA] + U methods[34,35]. Since the combination of DFT + DMFT techniques started to appear, a number of DC correction methods have been proposed[36–41]. However, it remains unclear which of these methods is best suited for the current system. Here, instead of examining each DC method, we take a different approach: we treat ε_{DC} as an adjustable parameter and, based on the experimental input, i.e., the ordered moment, determine the parameter range suitable for the material and then use it for the more detailed calculations of the quasi-particle weight.

The inset of Fig. 3(a [b]) shows the total (orbital-resolved) Ru d electron densities $N(N_\alpha)$ as a function of ε_{DC}. As one can see, the total density N remains larger than 3, the nominal value for Ru^{5+}, for the whole ε_{DC} range examined. To realize $N = 3$, i.e., the d^3 electron configuration, ε_{DC} must be unrealistically small. N and N_α are not

sensitive to the magnetic state, compare paramagnetic (PM) solutions and G-type antiferromagnetic (G-AFM) solutions. In all ε_{DC}, a_{1g} orbitals have electron density closer to 1 than e_g' orbitals. From this, one could anticipate that a_{1g} electrons contribute to magnetism more strongly than e_g' electrons.

In the inset of Fig. 3(a), we also plot the analytical line

$$\varepsilon_{DC} = U_{ave}\left(N - \frac{1}{2}\right) - \frac{1}{2}J_{ave}(N-1), \tag{1}$$

which is the so-called fully localized limit (FLL)[34], with U_{ave} and J_{ave} being averaged Coulomb interactions and exchange interactions computed from matrix elements presented in the Method section, Eqs (4) and (5), respectively. We notice that the analytic curve and the numerical data practically overlap at $\varepsilon_{DC} \gtrsim 15$ eV. Thus, if one takes the FLL DC correction and imposes the condition that impurity occupation N and the one in the DC correction Eq. (1) coincide, any point at $\varepsilon_{DC} \gtrsim 15$ eV fulfills this condition. This means that the full convergence for this scheme is very difficult. Instead, we take the Ru d occupancy from the DFT calculation, $N=4.3$, and use this value in Eq. (1) to obtain $\varepsilon_{DC}=15.92$ eV. This ε_{DC} gives impurity occupation $N=4.28(4.31)$ in the PM (G-AFM) solution at $T=348$ K. It is reported that the FLL formula gives a slightly larger impurity occupancy than the "nominal" DC (in this case $N=3$), which is close to the "exact" DC[41]. However, the true nominal occupancy in Ru d states is not known yet. While it remains to be justified, our results using the FLL DC with $N=4.3$, as discussed below, suggest that our choice of ε_{DC} provides a reasonable physical picture of $SrRu_2O_6$. It is very interesting to apply the improved DC correction to $SrRu_2O_6$, but this remains a future research.

Given the vital information on the Ru d occupation number N vs. ε_{DC} in the inset of Fig. 3(a), we examine physical quantities as a function of ε_{DC}. Figure 3(a) shows the total ordered moment $\langle M_z\rangle$ and orbital-resolved ordered moment $\langle M_{\alpha z}\rangle$ for G-AFM as a function of ε_{DC}. Here, $\langle M_z\rangle = \sum_\alpha \langle M_{\alpha z}\rangle$ with $\langle M_{\alpha z}\rangle = N_{\alpha\uparrow} - N_{\alpha\downarrow}$. One notices that the ordered moment on the a_{1g} orbital is larger compared to the e_g' orbitals. This is because the a_{1g} occupation is closer to one than the e_g' occupations [see the inset of Fig. 3(b)] and, therefore, the spin polarization is easily induced.

It is remarkable that the ordered moment varies drastically with ε_{DC}. This comes from the smaller occupation in a_{1g} orbitals than e_g' orbitals, i.e., $N_{a_{1g}} < N_{e_g'}$ [see Fig. 3(b) inset]. This is partly explained by DFT results; it is found that the bare a_{1g} level is about 0.3 eV higher than the e_g' level, and $N_{a_{1g}} = 1.42 < N_{e_g'} = 1.45$. However, the orbital polarization $N_{e_g'} - N_{a_{1g}}$ is found to be significantly enhanced in our DMFT calculations; from 0.03 in DFT to at most 0.25. This is because the orbital polarization is enhanced by correlations[42,43]. Furthermore, as shown later, spectral weight right below the Fermi level is dominated by a_{1g} orbital [Fig. 4(a)]. Since reducing ε_{DC} roughly corresponds to lowering E_F, a_{1g} orbital changes the occupation number more sensitively than e_g' orbitals, leading to the large suppression in the ordered moment with decreasing ε_{DC}.

With $\varepsilon_{DC}=15.92$ eV (the FLL DC correction with $N=4.3$), we found the ordered moment $\langle M_z\rangle = \sim 1.2\ \mu_B$. This value is consistent with the experimental observation $1.4\ \mu_B$[16,17], giving us confidence in our choice of ε_{DC}. This is quite different from the nominal occupation of Ru^{5+}, $N=3$. Such a large difference of N from its nominal value comes from the strong mixture between Ru d states and O p states in low-energy bands. It should be noted that in order to achieve $N=3$, one needs to adopt unphysically small ε_{DC}.

The strong sensitivity of $\langle M_z\rangle$ on ε_{DC} indicates the magnetism and the band structure are strongly coupled. This might suggest that $SrRu_2O_6$ is in the weak coupling regime despite relatively large values of the matrix elements of $\hat{U}$. But is this true? Thus, we now turn to the quasiparticle weight, which is the direct measure of the correlation strength. Figure 3(b) shows orbital dependent quasiparticle weight Z_α as a function of ε_{DC}. It is seen that Z_α for $\alpha = a_{1g}$ becomes extremely small at $\varepsilon_{DC} < 10$ eV and $\varepsilon_{DC} \sim 14$ eV approaching integer fillings $N=3$ and 4, respectively, while Z_α for $\alpha = e_g'$ remains larger than 0.02. This indicates that the correlation effect is quite strong and the system is in the vicinity of orbital-selective Mott insulating regimes[44], in which $\alpha = a_{1g}$ electrons tend to be localized but e_g' electrons maintain an itinerant character. This dichotomy between localized and itinerant characters will be discussed in detail later. We also note that the coexistence of localized and itinerant electrons would lead to the bad-metal behavior that has been suggested in an extended range of coupling and carrier densities in strongly-correlated multiorbital systems in the presence of Hund's coupling[45,46].

In many magnetic materials, the ordered moment increases with increasing correlation strength. Thus, the quasiparticle weight in a PM solution and the ordered moment in a magnetic solution tend to have a negative correlation. As shown in Fig. 3(a) and (b), on the contrary, the ordered moments become large where the quasiparticle weights become large, i.e., they have a positive correlation. All these observations suggest that $SrRu_2O_6$ is in the strong coupling regime, but Mott physics and itinerant band physics coexist.

Temperature dependence. Based on the detailed comparison with experiments, now we focus on $\varepsilon_{DC}=15.92$ eV and examine the temperature dependence of the electronic property of $SrRu_2O_6$.

We start from the low-temperature electronic property. Figure 4(a,b) show the Ru d density of states computed by the maximum entropy analytic continuation for the impurity Green's functions on the Matsubara axis[47]. e_g' states have a clear gap in both PM and G-AFM solutions with the peak-to-peak distance ~0.6 eV and ~0.9 eV, respectively. For a_{1g} states, the gap structure is rather vague especially in the PM solution. The minimum peak-to-peak distance is ~0.2 eV for both PM and G-AFM. These values are comparable to the experimental estimate on the activation energy ~0.4 eV[16].

Magnetic properties are summarized in Fig. 1(b). Local ordered moment $\langle M_z\rangle$ is computed for G-type AFM and plotted as a function of temperature. At a glance, one notices a close resemblance between the theoretical $\langle M_z\rangle$ vs. T curve and experimental ones reported in refs[16] and [17]. Theoretical results for the ordered moment at

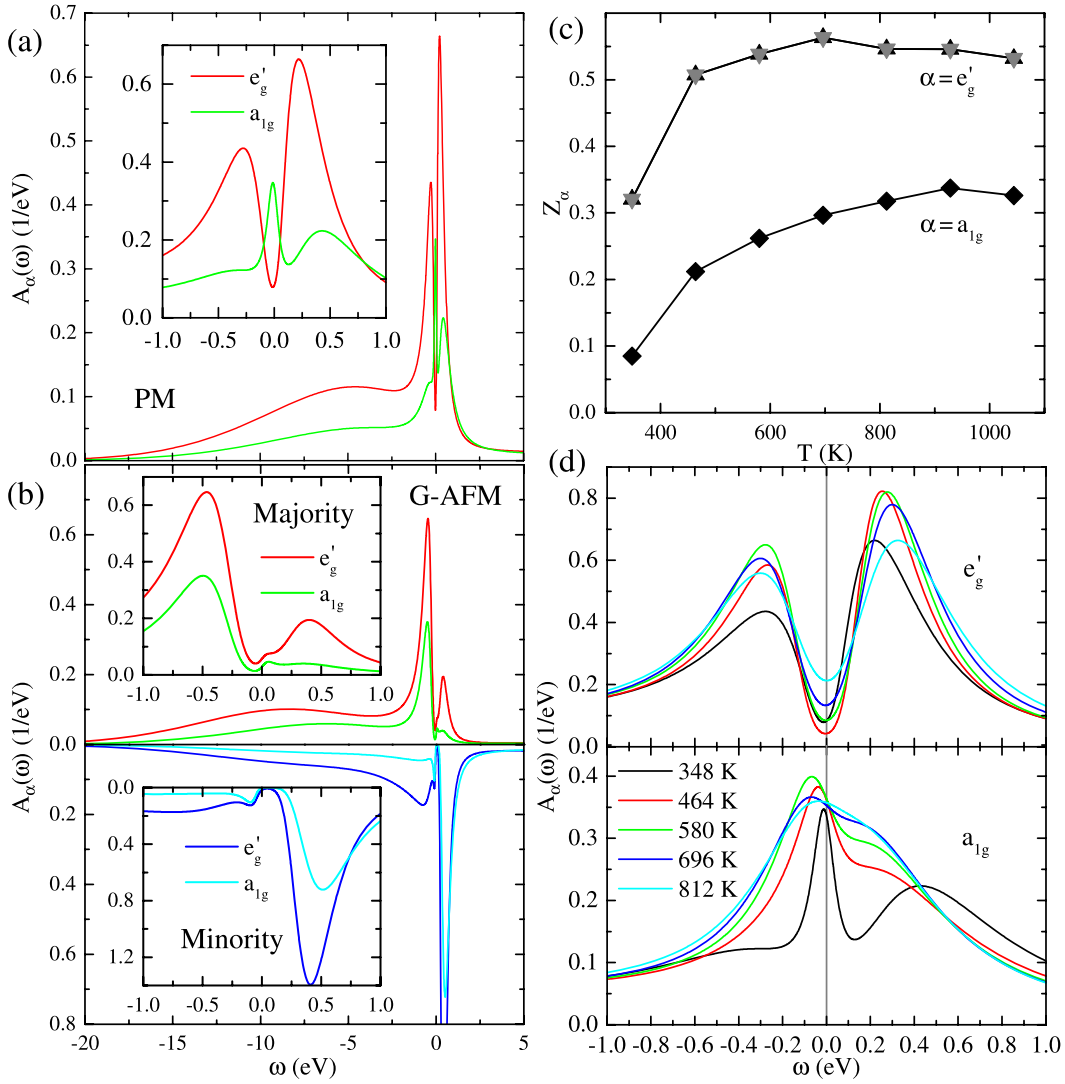

Figure 4. DMFT results of the spectral function $A_\alpha(\omega)$ for a PM phase (**a**) and a G-AFM phase (**b**) at $T = 348$ K. (**c**) Orbital-resolved quasiparticle wright Z_α as a function of T. The a_{1g} band shows a stronger mass enhancement than the e_g' band by a factor of 2–3. (**d**) Temperature dependent spectral function $A_\alpha(\omega)$.

low temperatures is $\langle M_z \rangle \sim 1.2\ \mu_B$ and the Néel temperature $T_N \sim 700$ K are reasonably close to the experimental results, $\langle M_z \rangle \sim 1.4\ \mu_B$ and $T_N \sim 565$ K. Theoretical T_N is overestimated by about 20%, which could be attributed to the mean field nature of the current "single-site" DMFT and the uniaxial anisotropy existing in real material due to the finite spin-orbit coupling but absent in our calculations.

In Slater-type systems in the weak coupling limit, local moments disappear when magnetic ordering disappears above T_N. On the other hand, in Mott insulators in the strong coupling limit, local moments remain unchanged above T_N. In the intermediate crossover regime, local moments decrease with increasing temperature but survive at high temperatures. We have also computed the equal-time spin-spin correlation in an impurity model $\langle M_z^2 \rangle$ by suppressing magnetic ordering and plotted in Fig. 1(b). It is remarkable that $\langle M_z^2 \rangle$ remains constant in the whole temperature range. From $\langle M_z^2 \rangle \approx 1.8\ \mu_B^2$ and using the spin rotational symmetry, the size of the local moment is deduced as $M = \sqrt{3\langle M_z^2 \rangle} \approx 2.3\ \mu_B$, which is roughly 2 times larger than the size of the ordered moment at low temperatures. Clearly $SrRu_2O_6$ is not in the weak-coupling limit and most likely in the strong-coupling limit. Similar dichotomy between large local moments and small ordered magnetic moments was theoretically suggested for iron-based superconductors[48,49] and has indeed been experimentally reported[50].

We also found other evidence of strong correlation effects from the temperature dependent quasiparticle weight. As shown in Fig. 4(c), Z_α in PM solutions are decreased with decreasing T. This behavior contradicts with what one expects for a good metal where the electron coherence is enhanced with decreasing temperature. It is also interesting to point out that the renormalization in $Z_{e_g'}$ is moderate for high temperatures. This is because e_g' bands maintain the band-insulator-like character and have larger spectral weights away from $\omega = 0$. On the other

hand, the renormalization in $Z_{a_{1g}}$ is significant. Thus, $SrRu_2O_6$ is in the vicinity of the correlation-induced orbital-selective Mott transition.

Our findings are remarkably different from the previous DFT + DMFT study on $SrRu_2O_6$. Reference[19] found a large Ru moment ~3 μ_B and an extremely high transition temperature ~2000 K. While sufficient details are not provided in ref.[19], we suspect from our calculations that the main difference arises from the inclusion of ligand O p states in our calculations that are crucial to describe the electronic properties of the late transition-metal oxides with deeper d levels.

As a closely related system, $SrTcO_3$ was studied in ref.[7]. The experimental ordered moment is found to be 2.13(1.87) μ_B at low (room) temperature. The ordered moment deduced by DFT is 1.3 μ_B. All these values are substantially smaller than $S = 3/2$ moment 3.87 μ_B. $SrTcO_3$ as well as $SrMnO_3$, both of which are d^3 systems, were examined using DFT + DMFT in ref.[8]. The ordered moment is found to be 2.5 μ_B for $SrTcO_3$ and 3 μ_B for $SrMnO_3$ at low temperatures. These values are close to the experimental values. The local moment for the two materials are estimated from $\langle S_{zi}^2 \rangle$ above T_N to be 2.7 μ_B for the Tc and 3.8 μ_B for Mn compound. The fluctuating magnetic moment of Mn is close to the maximal value 3.87 μ_B, while that for Tc is suppressed because of the more-itinerant nature of $SrTcO_3$. The reported dependence of ordered and local moments on the "B" site elements of perovskite $SrBO_3$ is consistent with the Slater-Mott crossover for half-filled Hubbard models. Our results on $SrRu_2O_6$ are closer to $SrTcO_3$ than $SrMnO_3$. However, the reduction from the local moment to the ordered moment is much stronger 1.3/23 ~ 0.57 for our $SrRu_2O_6$ as compared with 2.5/2.7 ~ 0.93 for $SrTcO_3$. This clearly indicates the importance of the coexistence of localized and itinerant electrons in $SrRu_2O_6$. It would be also very instructive to see the difference between $SrRu_2O_6$ and other ruthenium compounds with the nominal Ru valence of +5. Double perovskite ruthenates Ba_2LaRuO_6 ($T_N = 29.5$ K), Ca_2LaRuO_6 ($T_N = 12$ K)[51,52] and Sr_2YRuO_6 ($T_N = 26$ K)[51,53] are among such compounds. The high temperature fluctuating (low temperature ordered) moment of Ba_2LaRuO_6, Ca_2LaRuO_6 and Sr_2YRuO_6 was deduced as 4.00, 4.27 and 3.13 μ_B (1.96, 1.92 and 1.85 μ_B), respectively. These values are factor 1.4–1.8 larger than the corresponding values obtained in this study for $SrRu_2O_6$. The difference between these double perovskite ruthenates and $SrRu_2O_6$ can be ascribed to the more localized nature of the double perovskite ruthenates, in which Ru sites are separated by rare earth ions, and the Ru valence expected to be much closer to +5.

Discussion

In the previous sections, we discussed magnetic and electronic properties of $SrRu_2O_6$. Here we discuss some implications of our results to the transport property. Because of the large imaginary part of the self-energies, it remains challenging to identify the low-energy feature of the spectral function. Nevertheless, the temperature dependence of $A_\alpha(\omega)$ might give a hint. As shown in Fig. 4(d), e_g' bands show the gapped feature and, therefore, do not contribute to the transport much. On the other hand, the spectral function for the a_{1g} band is gradually diminished at $\omega \sim 0$ with decreasing temperature. Thus, we expect the electric resistivity $\rho(T)$ to increase with decreasing temperature in the whole temperature range, including $T \gg T_N$.

In the weak-coupling picture, $SrRu_2O_6$ is a band insulator at both above and below T_N, the gap amplitude is fixed at $T > T_N$ and grows rapidly according to the magnetic order parameter at $T < T_N$. Therefore, the $\rho(T)$ curve is expected to have a kink at T_N. On the other hand, in our strong coupling picture, the spectral functions evolve dynamically even in the PM regime. Due to the large self-energy or scattering rate, details of low-energy features in $A(\omega)$ are smeared out. Thus, $\rho(T)$ is expected to change smoothly across T_N.

To verify our results, it would be very important to experimentally examine the resistivity in the whole temperature range, from $T \ll T_N$ to $T \gg T_N$. Our preliminary results of the resistivity above room temperature appear to support this. Also, (angle resolved) photoemission spectroscopy measurements would provide direct evidence of the dynamical change in the spectral function, the evolution of the pseudogap feature to the full gap with decreasing temperature across T_N.

The current work suggests that $SrRu_2O_6$ has to be considered as a different class of material than a series of t_{2g}^3 TMOs, including $SrMnO_3$, $SrTcO_3$ and $NaOsO_3$, where the low-energy behavior is well captured by multi(3)-orbital Hubbard models. To understand the unique behavior of $SrRu_2O_6$, it is essential to consider strong hybridization between Ru d and O p states. This could largely modify the T vs. U phase diagram by reducing both T_N and the local moment M_{loc}, while the correlation strength in TM d states remains strong. There might be a large number of materials that could be classified into a similar category as $SrRu_2O_6$.

The main effect of the hybridization with O p states is driving the electron configuration of Ru to t_{2g}^4 rather than t_{2g}^3. In this respect, it would be very interesting to look for systems with the similar electron configurations as $SrRu_2O_6$ but stronger SOC. As discussed in ref.[54], the d^4 electron configuration would nominally imply an atomic moment $J = 0$, but, interatomic exchange can lead to the formation of a local moment and novel spin-orbital entangled magnetism.

To summarize, we have investigated the novel electronic and magnetic properties of the hexagonal compound $SrRu_2O_6$ using DFT + DMFT. The small moment on Ru ~1.2 μ_B and the relatively high Néel temperature ~700 K are consistent with the experimental report, ~1.4 μ_B and T_N ~ 565 K. These seemingly contradictory characters of $SrRu_2O_6$ are caused by the strong hybridization between Ru d states and ligand O p states, which increases the Ru d occupancy substantially from the nominal value 3. The strong Ru d-O p hybridization does not imply a weak-coupling nature. In fact, $SrRu_2O_6$ is in the strong-coupling regime, on the verge of the orbital-selective Mott localization. In contrast to the DFT results, a band insulator when magnetic ordering is suppressed, we predict that the electron spectral functions evolve dynamically with temperature. In particular above Néel temperature, the spectral functions exhibit pseudogap features, which turn to full gap with decreasing temperature. To verify our predictions, further experimental studies are desirable, including temperature dependent photoemission spectroscopy measurements and resistivity measurements.

Methods

DFT calculations were performed for the non-magnetic state with the Elk package[24] using the exchange-correlation functional proposed by Perdew *et al.*[55]. We considered the experimental lattice parameters and atomic configurations determined at room temperature[15].

Using the obtained band structure, we constructed the Wannier functions[26–29] containing the Ru t_{2g} and O p orbitals and calculated the transfer integrals among them. The energy window was set as $[-7.0{:}+1.0]$ eV. Further, we evaluated the interaction parameters, the Coulomb repulsion $\hat{U}$ and the exchange coupling $\hat{J}$, by the constrained random phase approximation (cRPA)[30]. In the calculation of the partially screened Coulomb interaction, we took 120 unoccupied bands and used a $4\times4\times4$ grid. The double Fourier transform of the constrained susceptibility was done with the cutoff of 5 (1/a.u.). We neglected the SOC since it is small compared with the Hund coupling constants.These calculations were performed using a density response code[56] recently developed for the Elk branch of the original EXCITING FP-LAPW code[24].

The obtained effective model consists of two parts as $H=H_{band}+\sum_{i\in \mathrm{Ru}}H_{int,i}$. The band part H_{band} is given by

$$H_{band}=\sum_{\vec{k},\sigma}\begin{bmatrix}\hat{d}^{\dagger}_{\vec{k}\sigma}, \hat{p}^{\dagger}_{\vec{k}\sigma}\end{bmatrix}\begin{bmatrix}\hat{\varepsilon}^{dd}_{\vec{k}}-\varepsilon_{DC}\hat{1} & \hat{\varepsilon}^{dp}_{\vec{k}}\\ \hat{\varepsilon}^{pd}_{\vec{k}} & \hat{\varepsilon}^{pp}_{\vec{k}}\end{bmatrix}\begin{bmatrix}\hat{d}_{\vec{k}\sigma}\\ \hat{p}_{\vec{k}\sigma}\end{bmatrix}. \tag{2}$$

Here, $\hat{d}_{\vec{k}\sigma}$ ($\hat{p}_{\vec{k}\sigma}$) is a vector consisting of annihilation operators of Ru t_{2g} (O p) electrons with spin σ in a momentum $\vec{k}$ space. The dispersion $\hat{\varepsilon}^{\alpha\beta}_{\vec{k}}$ consists of Wannier parameters, with α and β running through Ru t_{2g} and O p states. ε_{DC} for interacting Ru t_{2g} states is the DC correction.

The interaction part H_{int} is given by

$$\begin{aligned}H_{int} &= \sum_{a}U_{aa}d^{\dagger}_{a\uparrow}d_{a\uparrow}d^{\dagger}_{a\downarrow}d_{a\downarrow}+\sum_{a\neq b}U_{ab}d^{\dagger}_{a\uparrow}d_{a\uparrow}d^{\dagger}_{b\downarrow}d_{b\downarrow}\\ &+\sum_{a>b,\sigma}(U_{ab}-J_{ab})d^{\dagger}_{a\sigma}d_{a\sigma}d^{\dagger}_{b\sigma}d_{b\sigma}\\ &+\sum_{a\neq b}J_{ab}(d^{\dagger}_{a\uparrow}d_{b\uparrow}d^{\dagger}_{b\downarrow}d_{a\downarrow}+d^{\dagger}_{a\uparrow}d_{b\uparrow}d^{\dagger}_{a\downarrow}d_{b\downarrow}).\end{aligned} \tag{3}$$

Here, the index i for Ru sites is suppressed for simplicity. The matrix elements of $\hat{U}$ and $\hat{J}$, evaluated by using the cRPA, are given by

$$\hat{U}=\begin{bmatrix}5.236 & 4.260 & 4.196\\ 4.260 & 5.236 & 4.196\\ 4.196 & 4.196 & 5.482\end{bmatrix} \tag{4}$$

and

$$\hat{J}=\begin{bmatrix} & 0.488 & 0.567\\ 0.488 & & 0.567\\ 0.567 & 0.567 & \end{bmatrix} \tag{5}$$

in units of eV with the basis of $\{e'_{g1}, e'_{g2}, a_{1g}\}$.

Recently, we become aware of a preprint by Hariki *et al.* (Ref.[57]). They performed similar DFT+DMFT calculations with different interaction parameters and a DC scheme and obtained similar conclusion as Ref.[19].

References

1. Slater, J. C. Magnetic Effects and the Hartree-Fock Equation. *Phys. Rev.* **82**, 538 (1951).
2. Mott, N. F. The Basis of the Electron Theory of Metals, with Special Reference to the Transition Metals. *Proc. Phys. Soc., London, Sect. A* **62**, 416 (1949).
3. Hubbard, J. Electron Correlations in Narrow Energy Bands. *Proc. R. Soc., London, Sect. A* **276**, 238 (1963).
4. Anderson, P. W. Antiferromagnetism. Theory of Superexchange Interaction. *Phys. Rev.* **79**, 350 (1950).
5. Takeda, T. & Ōhara, S. Magnetic Structure of the Cubic Perovskite Type $SrMnO_3$. *J. Phys. Soc. Jpn.* **37**, 275 (1974).
6. Shi, Y. G. *et al.* Continuous metal-insulator transition of the antiferromagnetic perovskite $NaOsO_3$. *Phys. Rev. B* **80**, 161104(R) (2009).
7. Rodriguez, E. E. *et al.* High Temperature Magnetic Ordering in the 4*d* Perovskite $SrTcO_3$. *Phys. Rev. Lett.* **106**, 067201 (2011).
8. Mravlje, J., Aichhorn, M. & Georges, A. Origin of the High Néel Temperature in $SrTcO_3$. *Phys. Rev. Lett.* **108**, 197202 (2012).
9. Nganba Meetei, O., Erten, O., Randeria, M., Trivedi, N. & Woodward, P. Theory of High T_C Ferrimagnetism in a Multiorbital Mott Insulator. *Phys. Rev. Lett.* **110**, 087203 (2013).
10. Sleight, A. W., Gilson, J. L., Weiher, J. F. & Bindloss, W. Semiconductor-metal transition in novel $Cd_2Os_2O_7$. *Solid State Commun.* **14**, 357 (1974).
11. Mandrus, D. *et al.* Continuous metal-insulator transition in the pyrochlore $Cd_2Os_2O_7$. *Phys. Rev. B* **63**, 195104 (2001).
12. Yamaura, J. *et al.* Tetrahedral Magnetic Order and the Metal-Insulator Transition in the Pyrochlore Lattice of $Cd_2Os_2O_7$. *Phys. Rev. Lett.* **108**, 247205 (2012).
13. Shinaoka, H., Miyake, T. & Ishibashi, S. Noncollinear Magnetism and Spin-Orbit Coupling in 5*d* Pyrochlore Oxide $Cd_2Os_2O_7$. *Phys. Rev. Lett.* **108**, 247204 (2012).
14. Lifshitz, I. M. Anomalies of Electron Characteristics of a Metal in the High Pressure Region. *Sov. Phys. JETP* **11**, 1130 (1960).
15. Hiley, C. I. *et al.* Ruthenium(V) oxides from low-temperature hydrothermal synthesis. *Angew. Chem., Int. Ed.* **53**, 4423 (2014).
16. Tian, W. *et al.* High antiferromagnetic transition temperature of the honeycomb compound $SrRu_2O_6$. *Phys. Rev. B* **92**, 100404(R) (2015).
17. Hiley, C. I. *et al.* Antiferromagnetism at $T>500$ K in the layered hexagonal ruthenate $SrRu_2O_6$. *Phys. Rev. B* **92**, 104413 (2015).
18. Singh, D. J. Electronic structure and the origin of the high ordering temperature in $SrRu_2O_6$. *Phys. Rev. B* **91**, 214420 (2015).

19. Streltsov, S., Mazin, I. I. & Foyevtsova, K. Localized itinerant electrons and unique magnetic properties of $SrRu_2O_6$. *Phys. Rev. B* **92**, 134408 (2015).
20. Georges, A., Kotliar, G., Krauth, W. & Rozenberg, M. J. Dynamical mean-field theory of strongly correlated fermion systems and the limit of infinite dimensions. *Rev. Mod. Phys.* **68**, 13 (1996).
21. Anisimov, V. I., Poteryaev, A. I., Korotin, M. A., Anokhin, A. O. & Kotliar, G. First-principles calculations of the electronic structure and spectra of strongly correlated systems: dynamical mean-field theory. *J. Phys. Condens. Matter* **9**, 7359 (1997).
22. Lichtenstein, A. I. & Katsnelson, M. I. *Ab initio* calculations of quasiparticle band structure in correlated systems: LDA++ approach. *Phys. Rev. B* **57**, 6884 (1998).
23. Kotliar, G. *et al*. Electronic structure calculations with dynamical mean-field theory. *Rev. Mod. Phys.* **78**, 865 (2006).
24. Spitaler, J. *et al*. The EXCITING FP-LAPW code: http://exciting.sourceforge.net/.
25. Fatuzzo, C. G. *et al*. Spin-orbit-induced orbital excitations in Sr_2RuO_4 and Ca_2RuO_4: A resonant inelastic x-ray scattering study. *Phys. Rev. B* **91**, 155104 (2015).
26. Marzari, N. & Vanderbilt, D. Maximally localized generalized Wannier functions for composite energy bands. *Phys. Rev. B* **56**, 12847 (1997).
27. Souza, I., Marzari, N. & Vanderbilt, D. Maximally localized Wannier functions for entangled energy bands. *Phys. Rev. B* **65**, 035109 (2001).
28. Kuneš, J. *et al*. Wien2wannier: From linearized augmented plane waves to maximally localized Wannier functions. *Comput. Phys. Commun.* **181**, 1888 (2010).
29. Mostofi, A. A. *et al*. Wannier90: A Tool for Obtaining Maximally-Localised Wannier Functions. *Comput. Phys. Commun.* **178**, 685 (2008).
30. Aryasetiawan, F. *et al*. Frequency-dependent local interactions and low-energy effective models from electronic structure calculations. *Phys. Rev. B* **70**, 195104 (2004).
31. Werner, P., Comanac, A., De Medici, L., Troyer, M. & Millis, A. J. Continuous-Time Solver for Quantum Impurity Models. *Phys. Rev. Lett.* **97**, 076405 (2006).
32. Werner, P. & Millis, A. J. Hybridization expansion impurity solver: General formulation and application to Kondo lattice and two-orbital models. *Phys. Rev. B* **74**, 155107 (2006).
33. Haule, K. Quantum Monte Carlo impurity solver for cluster dynamical mean-field theory and electronic structure calculations with adjustable cluster base. *Phys. Rev. B* **75**, 155113 (2007).
34. Czyzyk, M. T. & Sawatzky, G. A. Local-density functional and on-site correlations: The electronic structure of La_2CuO_4 and $LaCuO_3$. *Phys. Rev. B* **49**, 14211 (1994).
35. Anisimov, V. I., Aryasetiawan, F. & Lichtenstein, A. I. First-principles calculations of the electronic structure and spectra of strongly correlated systems: the LDA+*U* method. *J. Phys. Condens. Matter* **9**, 767 (1997).
36. Lichtenstein, A. I., Katsnelson, M. I. & Kotliar, G. Finite-Temperature Magnetism of Transition Metals: An *ab initio* Dynamical Mean-Field Theory. *Phys. Rev. Lett.* **87**, 067205 (2001).
37. Amadon, B. *et al*. Plane-wave based electronic structure calculations for correlated materials using dynamical mean-field theory and projected local orbitals. *Phys. Rev. B* **77**, 205112 (2008).
38. Haule, K., Yee, C.-H. & Kim, K. Dynamical mean-field theory within the full-potential methods: Electronic structure of $CeIrIn_5$, $CeCoIn_5$, and $CeRhIn_5$. *Phys. Rev. B* **81**, 195107 (2010).
39. Kuneš, J. *et al*. Spin State of Negative Charge-Transfer Material $SrCoO_3$. *Phys. Rev. Lett.* **109**, 117206 (2012).
40. Haule, K., Birol, T. & Kotliar, G. Covalency in transition-metal oxides within all-electron dynamical mean-field theory. *Phys. Rev. B* **90**, 075136 (2014).
41. Haule, K. Exact Double Counting in Combining the Dynamical Mean Field Theory and the Density Functional Theory. *Phys. Rev. Lett.* **115**, 196403 (2015).
42. Okamoto, S. & Millis, A. J. Electron-lattice coupling, orbital stability, and the phase diagram of $Ca_{2-x}Sr_xRuO_4$. *Phys. Rev. B* **70**, 195120 (2004).
43. Werner, P. & Millis, A. J. High-Spin to Low-Spin and Orbital Polarization Transitions in Multiorbital Mott Systems. *Phys. Rev. Lett.* **99**, 126405 (2007).
44. de' Medici, L., Hassan, S. R., Capone, M. & Dai, X. Orbital-Selective Mott Transition out of Band Degeneracy Lifting. *Phys. Rev. Lett.* **102**, 126401 (2009).
45. de' Medici, L., Mravlje, J. & Georges, A. Janus-Faced Influence of Hund's Rule Coupling in Strongly Correlated Materials. *Phys. Rev. Lett.* **107**, 256401 (2011).
46. Georges, A., de' Medici, L. & Mravlje, J. Strong Correlations from Hund's Coupling. *Annu. Rev. Condens. Matter Phys.* **4**, 137 (2013).
47. Jarrell, M. & Gubernatis, J. E. Bayesian inference and the analytic continuation of imaginary-time quantum Monte Carlo data. *Physics Reports* **269**, 133 (1996).
48. Hansmann, P. *et al*. Dichotomy between Large Local and Small Ordered Magnetic Moments in Iron-Based Superconductors. *Phys. Rev. Lett.* **104**, 197002 (2010).
49. Toschi, A., Arita, R., Hansmann, P., Sangiovanni, G. & Held, K. Quantum dynamical screening of the local magnetic moment in Fe-based superconductors. *Phys. Rev. B* **86**, 064411 (2012).
50. Liu, M. *et al*. Nature of magnetic excitations in superconducting $BaFe_{1.9}Ni_{0.1}As_2$. *Nature Phys.* **8**, 376 (2012).
51. Greatrex, R., Greenwood, N. N., Lal, M. & Fernandez, I. A study of the ruthenium(V) perovskites M_2LnRuO_6(M = Ca, Ln = Y, La, or Eu; M = Sr, Ln = Y; M = Ba, Ln = La or Eu) by ^{99}Ru Mössbauer spectroscopy and other techniques. *J. Solid State Chem.* **30**, 137 (1979).
52. Battle, P. D., Goodenough, J. B. & Price, R. The crystal structures and magnetic properties of Ba_2LaRuO_6 and Ca_2LaRuO_6. *J. Solid State Chem.* **46**, 234 (1983).
53. Battle, P. D. & Macklin, W. J. The crystal and magnetic structures of Sr_2YRuO_6. *J. Solid State Chem.* **52**, 138 (1984).
54. Svoboda, C., Randeria, M. & Trivedi, N. Effective magnetic interactions in spin-orbit coupled d^4 Mott insulators. *Phys. Rev. B* **95**, 014409 (2017).
55. Perdew, J. P. & Wang, Y. Accurate and simple analytic representation of the electron-gas correlation energy. *Phys. Rev. B* **45**, 13244 (1992).
56. Kozhevnikov, A., Eguiluz, A. & Schulthess, T. *SC*'10 Proceedings of the 2010 ACM/IEEE International Conference for High Performance Computing, Networking, Storage, and Analysis (IEEE Computer Society, Washington, DC, 2010), pp. 1–10 (2010).
57. Hariki, A., Hausoel, A., Sangiovanni, G., & Kuneš, J. DFT+DMFT study on soft moment magnetism and covalent bonding in $SrRu_2O_6$, arXiv:1706.00328.

Acknowledgements

The research by S.O. and J.Y. is supported by the U.S. Department of Energy, Office of Science, Basic Energy Sciences, Materials Sciences and Engineering Division. This work was supported by JSPS KAKENHI Grants No. 15K17724 (M.O.) and 15H05883 (R.A.). N.T. acknowledges funding from DOE BES Grant DE-FG02-07ER46423. This research was initiated at the Kavli Institute for Theoretical Physics (KITP), the University of California,

Santa Barbara, where three of the authors (S.O., R.A. and N.T.) attended the program "New Phases and Emergent Phenomena in Correlated Materials with Strong Spin-Orbit Coupling." S.O., R.A. and N.T. thank the KITP, which is supported in part by the National Science Foundation under Grant No. NSF PHY11-25915, for hospitality.

Author Contributions

S.O. and N.T. conceived the project, S.O. performed the DMFT calculations, M.O. and R.A. performed the DFT calculations, S.O. and N.T. wrote the manuscript, and J.Y. provided experimental input. All the authors discussed the results.

Additional Information

Competing Interests: The authors declare that they have no competing interests.

Publisher's note: Springer Nature remains neutral with regard to jurisdictional claims in published maps and institutional affiliations.